Department of Sustainability
Division Models and technologies for Risks Reduction

Project: “Renewable energy potential maps for Lesotho”

Final report on solar radiation map production

Deliverable: WP2.D3

31th March 2020

AUTHORS

Lina Vitali (lina.vitali@enea.it)

Massimo D’Isidoro (massimo.disidoro@enea.it)

Gino Briganti (gino.briganti@enea.it)

Department of Sustainability
Division Models and technologies for Risks Reduction

1 INTRODUCTION

In the framework of the Project "Renewable energy potential maps for Lesotho" started in March 2018 and completed in March 2020, the activities defined in the Work Package 2 (WP2) aim at producing PhotoVoltaic (PV) energy potential map over Lesotho, by means of the numerical atmospheric model WRF (Weather Research and Forecasting).

The activities, planned and actually carried out within WP2, can be divided in three phases.

During the first one, a general overview and preliminary processing of collected meteorological observations (focussing on solar radiation and wind data) over Lesotho was done, in order to select the period to be used for model tuning. The analysis suggested the selection of year 2015, being the one maximising as much as possible the availability of hourly observations of wind and solar radiation, to be used for the comparison with model outcomes. The results of this activity were illustrated in detail in the report WP2.D1 due as a deliverable of the Project at the end of September 2018.

The second part of the work carried out within WP2 was related to the model tuning process consisting in simulating year 2015 with different WRF setups. More in details, different parameterizations affecting solar and wind energy outputs (cloud parameterization, radiation, planetary boundary layer) were tested and the simulations outcomes were compared to observations to establish the best performing model configuration. The chosen setup was used for the elaboration of the preliminary solar photovoltaic potential map, which was delivered in hardcopy format to the Lesotho authorities in February 2019 and illustrated in the report WP2.D2 due as a deliverable of the Project at the end of March 2019.

During the third and final phase of the Project, an effort was made to perform a multi-annual meteorological simulation in order to make available a climatological series of solar radiation fields to be used for photovoltaic energy assessment. More in details, a thirty years period (from 1989 to 2018) was simulated by means of WRF meteorological model, using the best performing model setup, as pointed out in the framework of WP2.D2 outcomes. Then PV energy assessment was carried out with the same spatial and temporal both coverage and resolution, in order to build the final version of the PV energy potential map for Lesotho.

This report, deliverable WP2.D3, presents the activities and the outcomes of the third and final phase of the Project. In section 2 a comprehensive presentation of the thirty years WRF meteorological simulation over Lesotho is provided. Section 3 is devoted to the description of solar radiation map production: methodologies used for the assessment are presented and the final outcome of WP2, i.e. the solar radiation map, is shown along with several additional products computed in the framework of the Project and made available into the WebGIS Data Base, developed as the final outcome of the Work Package 4. Finally some conclusions are drawn in section 4.

2 THIRTY YEARS WRF METEOROLOGICAL SIMULATION

In order to perform the renewable energy potential estimation over Lesotho, the WRF (Skamarock and Klemp, 2008) model in its WRF-SOLAR (Jimenez *et al.*, 2016; Lee *et al.*, 2017; Haupt *et al.*, 2018) version was used, which maintains all the features of WRF as Numerical Weather Prediction model, that is the prognosis of the typical meteorological fields (temperature, wind , pressure, etc.), and in addition contains some improvements in physical parameterisations concerning radiation-cloud interaction. Moreover, WRF-SOLAR provides directly in output quantities that are useful for solar energy applications such as global irradiance on horizontal surface, direct and diffuse irradiance. These features allowed us to use the same model version to produce both wind and PV potential estimations, the former extensively described in WP1.D3. For model details we refer to literature and to WP1.D2 deliverable.

In order to obtain PV energy estimation that is representative of the meteorological conditions temporal variability, a thirty years simulation covering period 1989-2018 was conducted using WRF settings derived in WP2.D2 and reported in Table 1.

PARAMETERISATION TYPE	SETTINGS
Long wave	RRTMG (4)
Short Wave	RRTMG (4)
Surface Layer	MM5 similarity (91)
Planetary Boundary Layer	Yonsei University scheme (1)
Microphysics	WRF Single Moment 5-class (4)
Land Surface Model	Noah (2)

TABLE 1: WRF PARAMETERISATIONS SETTING FOR THE THIRTY YEARS SIMULATION (1989-2018) CONDUCTED OVER LESOTHO. IN BRACKETS ARE THE NUMBERS CORRESPONDING TO THE MODEL NAMELIST SELECTION (NATIONAL CENTRE FOR ATMOSPHERIC RESEARCH (NCAR), 2014)).

The model was run using three nested domains with two-way nesting at horizontal resolutions of 15, 3 and 1 km, respectively. The parent domain was forced by 3 hourly ECMWF ERA5 (European Centre for Medium Range Weather Forecasts, 2020) reanalysis fields at 0.3° resolution. Table 2 summarises the three domains, while Figure 1 depicts the model domains locations and orography.

	D01	D02	D03
Resolution (km)	15	3	1
Number of points in longitude	85	211	256
Number of points in latitude	66	191	274
Number of vertical levels	41	41	41

TABLE 2: RESOLUTION (KM) OF THE THREE NESTED DOMAINS (D01, D02 AND D03) AND NUMBER OF GRID-POINTS IN LONGITUDE, LATITUDE AND VERTICAL LEVELS).

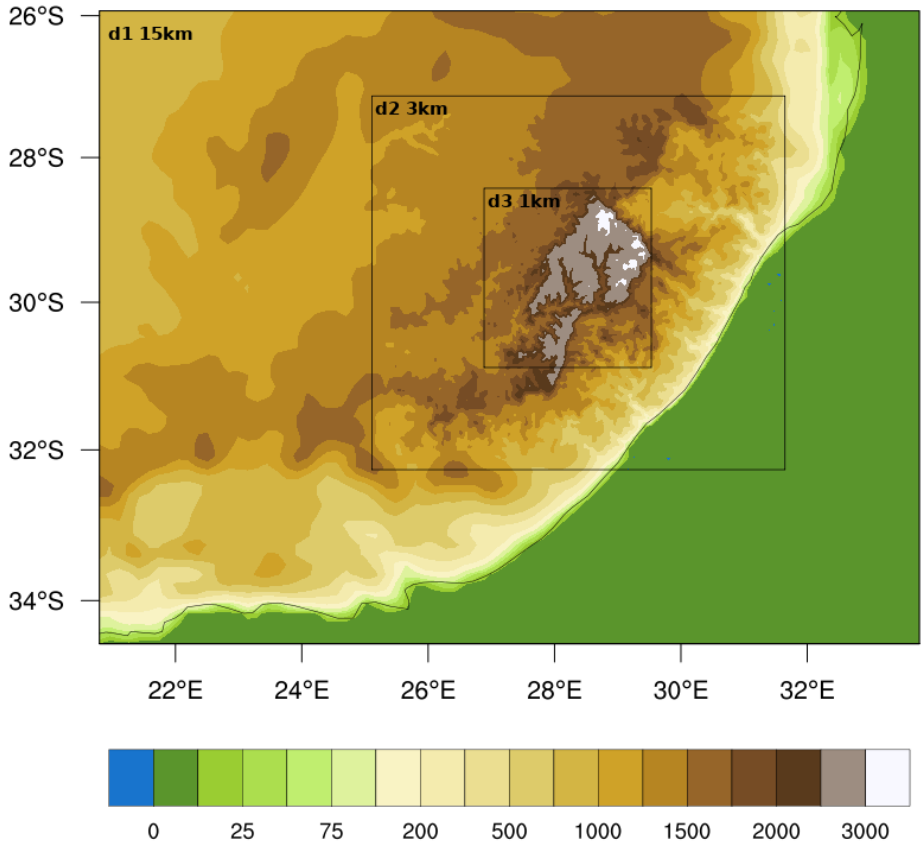

FIGURE 1: WRF NESTED DOMAINS LOCATION AND OROGRAPHY.

The modelling chain consisted of 30 hours simulations restarted every day at 18UTC using ERA5 on the parent domain, considering the initial 6 hours as spin-up period. Then, hourly model outputs of the following day from 00UTC to 23UTC are retained every day. This modelling setup was run using 192 cores on ENEA HPC CRESCO (Ponti *et al.*, 2014) facility. One year simulation took about 25 days CPU time and approximately 2TB data occupation (including data in input and

output) on the high performance filesystem connected to the machine, with a total of 60TB. The 30 hours simulations are independent each other and thanks to the CRESCO computing power capability (~10,000 cores) it was possible to perform all the period in few months, running more days in parallel, even considering the queue manager system allocating the resources to all the daily CRESCO users.

WRF outputs were post-processed to obtain hourly values of the quantities needed for photovoltaic energy computations. The "WRF-python" (Ladwig, 2017) and NCO (Zender, 2008) tools were used in order to retrieve the needed fields.

3 SOLAR RADIATION MAP PRODUCTION

The availability of the meteorological fields, produced by WRF simulations and covering a thirty years period (1989-2018), made it possible to perform energy assessment with the same spatial and temporal both coverage and resolution.

As a first step, solar radiation has been evaluated for the whole thirty years period, at hourly time resolution, and for every grid point of the domain covering Lesotho at 1 km spatial resolution.

Starting from this comprehensive and detailed data set, several elaboration can be performed. Integrating hourly data over the time it is possible to obtain the energy produced in the desired time interval (daily, monthly, yearly). In particular hourly data were integrated on an yearly basis, obtaining annual accumulated energy estimation for each of the thirty available years. Finally some statistics were performed. In particular the average value, based over the thirty annual outcomes, provides the best estimation of mean annual energy production, being thirty years a long period, statistically representative. Minimum and maximum values along with the standard deviation provide an estimation of the range and the inter annual variability of annual energy production to be expected.

Daily modulation and yearly variability of energy assessment were investigated too, by means of heatmaps elaboration, thus allowing, for each point of the domain, a quick identification of the period both of the year and of the day with maximum energy availability.

In this section, methodologies used for solar radiation map production are described, starting from the basic formulas used for hourly energy assessment for every grid point of the domain.

The final outcome of this Work Package, i.e. the solar radiation map, is then presented along with several additional products computed in the framework of the Project and made available into the WebGIS Data Base (deliverable WP4.D2).

3.1 Methodologies for solar radiation map production

3.1.1 Evaluation of global solar radiation incident on a tilted surface

The global solar radiation incident on a tilted surface can be estimated as the sum of three components: the beam (or direct) radiation G_b, coming directly from the sun; the diffuse radiation G_d, reaching the panel after being scattered by atmospheric compounds (water vapour, N_2, O_2, etc.),

dust particles or pollution in the atmosphere; the reflected radiation G_r, hitting the panel after being reflected from the ground, the adjacent surfaces and the nearby obstacles (e.g (La Gennusa *et al.*, 2007; Maleki, Hizam and Gomes, 2017).

We started from WRF output fields - ground albedo (ρ) and hourly radiation data (direct, direct normal and diffuse radiation on the horizontal surface, I_b, I_n and I_d, respectively) - and we assumed diffuse radiation being uniformly and isotropically distributed over the sky dome (according to Liu and C. Jordan, 1962) and PV modules being set in the optimal configuration, i.e. facing the equator. For every grid point (with latitude absolute value equal to L) total solar radiation G has been evaluated, at hourly time step, using the following equations.

$$G = G_b + G_d + G_r$$

$$G_b = I_n \left(sin(L - \beta)\, sin(\delta) + cos(L - \beta)\, cos(\delta)\, cos(h)\right)$$

$$G_d = I_d \left(1 + cos(\beta)\right)/2$$

$$G_r = (I_b + I_d)\, \rho \left(1 - cos(\beta)\right)/2$$

Beside L, the other angles in the formulas are β (the PV module inclination), δ (solar declination) and h (hour angle).

Concerning β, the module inclination with respect to the horizontal plane, its best value, maximizing the annual energy production, was computed by means of an optimization procedure and made available as an additional product in the framework of the Project. Details on the applied approach and on the related outcomes (i.e. the map of the optimum β values over Lesotho country) will be presented in section 3.4.

The solar declination δ is the angle between the equatorial plane and a line drawn from the centre of the earth to the centre of the sun. If the Earth were not tilted on its axis of rotation, the declination angle would always be 0°. Due to the Earth axis tilt, δ varies seasonally alongside the rotation of the Earth around the sun and vanishes at equinox days; therefore it can be expressed as a function of the day of the year. Several formulations are available in literature to describe this dependency. Here, one of the most frequent was applied. More in details, for the n-th day of the year, the declination δ was calculated as:

$$\delta = 23.45\, sin\left(360\, ((284+n)/365)\right)$$

The hour angle h is the angular distance of the sun with respect to its position at noon. Its formulation basically converts the local solar time into the number of degrees the sun moves across the sky (15° per hour). Indeed, the hour angle h was calculated using the true solar time t_{st} which differs from the conventional time t_c, by the deviation due to the actual longitude, the equation of time E_t and the 'daylight savings' time gap t_{leg}.

$$h=15\ (12 - t_{st})$$

$$t_{st} = (60\ t_c + 4\ (\ Lon - Lon_{\ TZ}) + E_t + 60\ t_{leg})/60$$

$$E_t = -9.87\ sin\ [2g\ (n - 81)] + 7.67\ sin[g\ (n - 1)]$$

with:

Lon = longitude of the site

$Lon_{\ TZ}$ = longitude of the reference meridian for the time zone

$g = 360°/365$

3.1.2 Factors influencing energy conversion efficiency of a PV system: basic fundamentals

The amount of solar radiation G, reaching the PV modules, is the most important factor in defining energy production of a PV system, but there are other factors that are important too. The power output (P) of the system depends on its conversion efficiency which of course has to be evaluated in order to better support energy exploitation planning.

The energy conversion efficiency of a PV system depends on a number of different external factors. Some of them are objective factors, mainly depending on meteorological conditions and module type. Among them the most important are:

- the "technology", that is the ability of the PV panel to catch the most part of the solar spectrum;
- the spectrum of the incoming light;
- the temperature of the PV module, which in turn depends on air temperature, light intensity and wind speed;
- the reflectivity of the module surface.

Some other effects are not intrinsic to the module type and it can be difficult to evaluate them a priori. The reason is they depend on how the modules are installed and then maintained and cleaned. Among them the most important are:

- possible partial shadowing, depending on local features and on the exact way the modules are installed;
- snow coverage, depending on how often it snows but also on how long the snow stays on the modules before melting or sliding off;
- dust and dirt deposition, depending on how much dust is in the air but also on how long it stays on the modules, that in turn depends on rainfall occurrences, the inclination of the modules and of course if the modules are cleaned from time to time.

Moreover, given the PV power delivered at the connectors of the module, before the power arrives at the grid, several electricity and heat losses (inverter efficiency, cables and transformer losses, and so on…) can be experienced by the system.

In addition the power production of a PV system tends to decrease slowly with system age. Literature (Jordan and Kurtz, 2013) found that PV modules typically lose about 0.5% of power per year of operation. If we consider an expected lifetime of the system of 20 years, an average loss of about 5% could be considered.

3.1.3 A priori analysis of PV energy conversion efficiency: factors taken into account

In the framework of the Project only objective factors were taken into account in evaluating energy conversion efficiency and therefore in estimating PV power output.

Indeed, factors depending on specific installation and maintenance features cannot be a priori evaluated and so they could not be considered in the context of the present ex-ante evaluation.

Concerning system and ageing losses, also these effects cannot be taken into account in an a priori assessment, since useful information to calculate them rely on the end-user system configuration; therefore a posteriori expert judgment is needed. Anyway a value of 14% can be applied by the end-user as a first approximation of the reduction of system efficiency due to both system and ageing losses. This value is recommended by JRC in the framework of the development of Photovoltaic Geographical Information System (PVGIS); please see JRC (2020) for more details.

Summarizing, the only effects considered in estimating the actual PV power output were the objective ones, depending only on meteorological conditions and module type. More exactly, only the reflectivity of the module surface and its temperature were considered. The change of system efficiency with variations in the spectrum of the sunlight was not considered. Indeed, information about the spectrum of the incoming sunlight was not available and, anyway, according to Photovoltaic Geographical Information System outcomes, this effect turned out to be negligible in the area of study (JRC, 2020).

Since both the reflectivity of the module surface and its temperature depend on time, position and meteorological conditions, both of them were on-line evaluated in function of time and space, at hourly time step for the whole thirty years period, and for every grid point of the domain covering Lesotho a 1 km resolution.

Methodologies used for evaluating these two effects are briefly described in the following sections.

3.1.4 The effect of module temperature on PV energy conversion efficiency

One of the most important factors influencing PV energy conversion efficiency is the temperature of the module. Generally, the efficiency decreases with increasing temperature, and the strength of this effect depends on the PV technology. Different approaches are used to describe PV efficiency, starting from the traditional linear expression, proposed by Evans and Florschuetz (1977) and still commonly used (e.g. Reis *et al.*, 2010; De Felice *et al.*, 2019), to the non-linear approaches; some examples are given in the inter-comparison outcomes of Friesen *et al.* (2007) and in the review of Dubey *et al.* (2013).

While the simple approach of Evans and Florschuetz (1977) was applied in the framework of the deliverable WP2.D2, for the final solar radiation map production the state-of-the-art approach, proposed by Huld *et al.* (2011) and deeply described in Huld and Gracia Amillo (2015), was adopted. This model was chosen because of its widespread usage and its good performances attained for several different PV technologies. Therefore, the effect of module temperature on the power output (P) was computed as follows:

$$P(G', T') = G' P_{STC} \left(1 + k_1 \ln(G') + k_2 \left(\ln(G')\right)^2 + k_3 T' + k_4 T' \ln(G') + k_5 T' \left(\ln(G')\right)^2 + k_6 T'^2\right)$$

$$G' \equiv \frac{G}{1000\ \mathrm{W.m^{-2}}}$$

$$T' \equiv T_{mod} - 25°C$$

Where G is the total solar radiation (computed as described in section 3.1.1) , P_{STC} is the power of the system operating in Standard Test Conditions (radiation G_{STC}=1000 W/m^2, module temperature T_{STC}=25°C; light spectrum equal to the global spectrum given in IEC 60904-3), T_{mod} is the actual module temperature and the coefficients k_i depend on module types. Assuming crystalline silicon (c-Si) modules, k_i were set according to Huld and Gracia Amillo (2015).

The module temperature (T_{mod}) depends in turn on the ambient temperature (T_{amb}), the radiation (G) and the wind speed (v). Numerous models have been proposed to describe this dependency (King, Kratochvil and Boyson, 2004; Faiman, 2008; Skoplaki and Palyvos, 2009; Reis *et al.*, 2010; Koehl *et al.*, 2011).

Here the module temperature was calculated according to Faiman (2008)

$$T_{mod} = T_{amb} + \frac{G}{U_0 + U_1 v}$$

The two coefficients U_0 and U_1 were chosen as in Huld and Gracia Amillo (2015) for c-Si modules.

3.1.5 The effect of module surface reflectivity on PV energy conversion efficiency

Since the surface of a PV module reflects part of the incident radiation, energy conversion efficiency depends on the reflectivity of the module surface. The module reflectivity depends in turns on the angle at which the incoming light hits the module surface. Generally, when the solar radiation hits the module at an angle away from the normal to the module surface, the reflectivity is increased and, as a consequence, energy conversion efficiency decreases, since reflected radiation does not contribute to the power output.

This effect was taken into account following Martin and Ruiz (2002, 2013) approach. According to their formulation, the effects on the three components of the incident radiation - beam (or direct), diffuse and reflected - were treated separately. More in detail reflectivity loss was taken into account substituting each of the three terms (in the equations of section 3.1.1) with a lowered quantity.

$G_b \rightarrow G_b \times (1 - F_B)$

$G_d \rightarrow G_d \times (1-F_D)$

$G_r \rightarrow G_r \times (1\text{-}F_R)$

where F_B, F_D and F_R represent the fractions of radiation lost due to reflectivity and they were evaluated according to the following equations.

$$F_B(\alpha) \equiv \frac{\exp(-\cos\alpha/a_r) - \exp(-1/a_r)}{1 - \exp(-1/a_r)}$$

$$F_D(\beta) \equiv \exp\left[-\frac{1}{a_r}\left(c_1\left(sin\beta + \frac{\pi - \beta - sin\beta}{1 + cos\beta}\right) + c_2\left(sin\beta + \frac{\pi - \beta - sin\beta}{1 + cos\beta}\right)^2\right)\right]$$

$$F_R(\beta) \equiv \exp\left[-\frac{1}{a_r}\left(c_1\left(sin\beta + \frac{\beta - sin\beta}{1 - cos\beta}\right) + c_2\left(sin\beta + \frac{\beta - sin\beta}{1 - cos\beta}\right)^2\right)\right]$$

where β is the module inclination with respect to the horizontal plane (as defined in section 3.1.1), α is the angle of incidence of solar radiation, a_r is the angular losses coefficient (an empirical dimensionless parameter depending on module technology), $c_1 = 4/3\pi$ and c_2 is a fitting parameter. Both a_r and c_2 were set according to Martin and Ruiz (2001).

3.1.6 Final photovoltaic map elaboration: thirty years statistical evaluation

Figure 2 presents the workflow of the elaborations carried out in order to get period evaluation from hourly one. Both total solar radiation (G) and power output (P) assessment was carried out at hourly time step, according to the formulations described in sections 3.1.1-3.1.5. Integrating hourly data on an yearly basis, annual accumulated energy evaluation was obtained for each of the thirty years. Finally some statistics over the thirty annual values were computed. In particular the final outcome of this Work Package, i.e. the solar radiation map, was obtained as the average of the thirty annual photovoltaic power output fields.

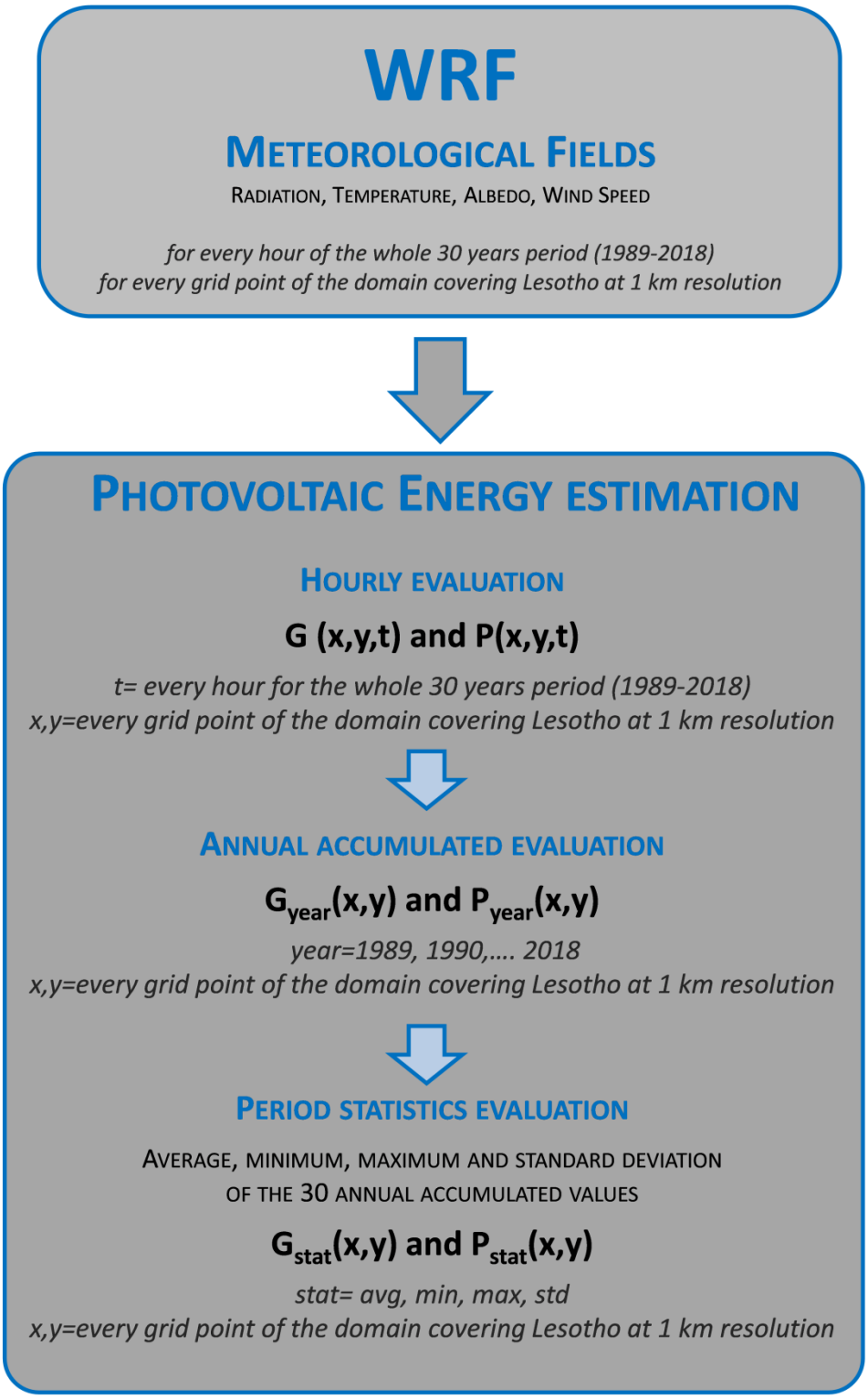

FIGURE 2: FROM HOURLY TO PERIOD EVALUATION: WORKFLOW OF THE ELABORATIONS

3.2 Photovoltaic power potential map

In Figure 3 the final outcome of this Work Package, i.e. the photovoltaic power potential map for Lesotho, is presented. Photovoltaic power values calculated at hourly time step - $P(x,y,t)$ - were integrated over each of the thirty years and then the thirty values were averaged obtaining mean yearly energy production, $P_{avg}(x,y)$, based on thirty years meteorological data. Figure 3 shows the energy data distribution pattern; a more detailed version of the final map together with a general description is attached in Annex A (the same document has been delivered as 180 hard copies at the end of February 2020) .

Results are expressed in kWh/kWp; namely energy production (kWh) has been normalized to the peak power of the PV system (kWp), i.e. the power of the system operating in Standard Test Conditions (STC), as defined in section 3.1.4.

It is worth noting that Lesotho presents a good PV production potential, ranging from 2020 to 2240 kWh/kWp, and low variability countrywide. The highest values are expected in the highlands, in particular in the Thaba Tseka and Mokhotlong districts, while the lowest ones are observed in the foothills. In general, PV power field reflects the spatial pattern of global radiation field (see section 3.3.1) but, obviously, here radiation spatial features turn out to be enhanced or smothered by temperature ones.

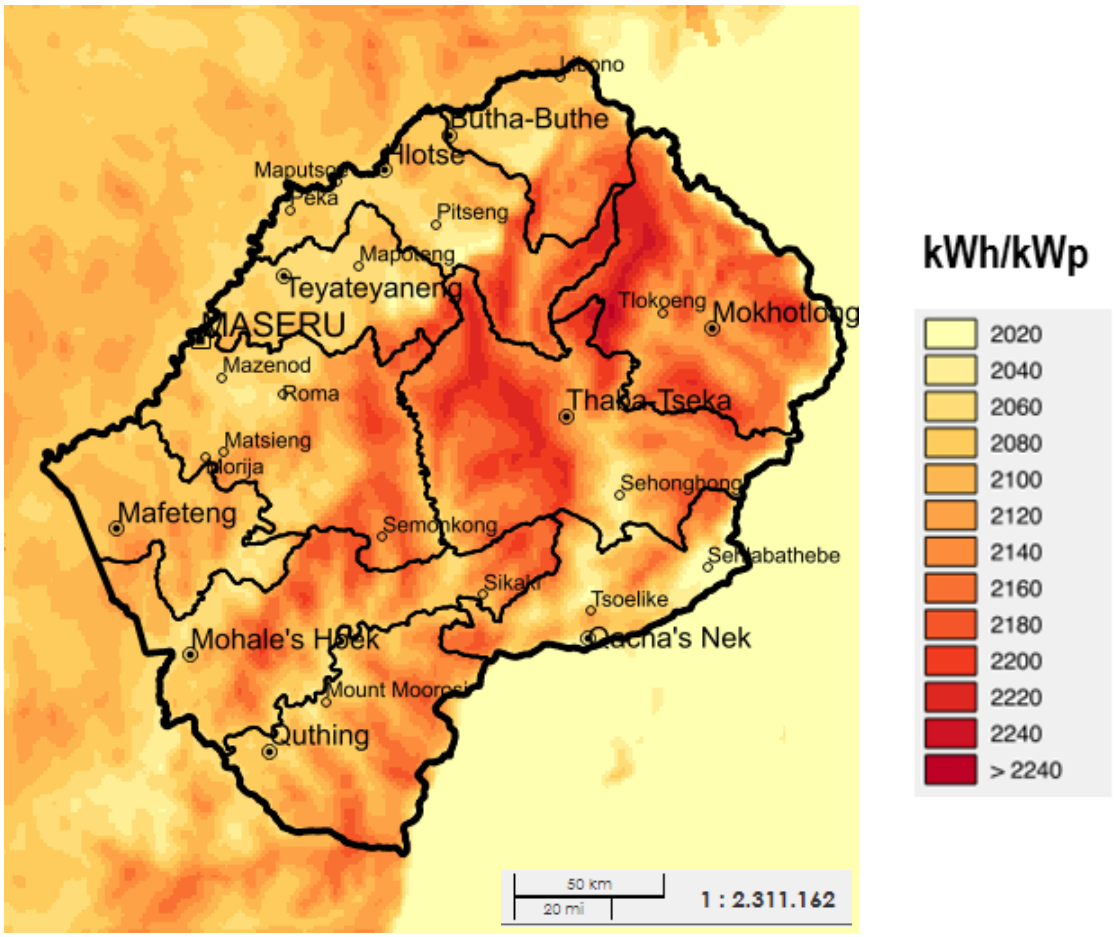

FIGURE 3: FINAL PHOTOVOLTAIC POWER POTENTIAL MAP FOR LESOTHO(kWh/kWp)

In order to provide an estimation of the range and the inter-annual variability of the annual energy production to be expected, in Figure 4 minimum and maximum values [$P_{min}(x,y)$ and $P_{max}(x,y)$] evaluated for every grid point of the domain over the thirty annual values, are presented along with the standard deviation outcomes [$P_{std}(x,y)$].

Minimum and maximum energy potential maps (top panels in Figure 4) present the same pattern as the average one (Figure 3). Moreover it is worth noting that the same values classification was used for all the three maps, pointing out that the same range of values can describe both spatial and inter-annual variability. The small inter-annual variability is confirmed by the low values of standard deviation outcomes (bottom left panel in Figure 4). In the context of general low values the higher variability turned out to be located in the foothills area and in the north-east boundary of the country.

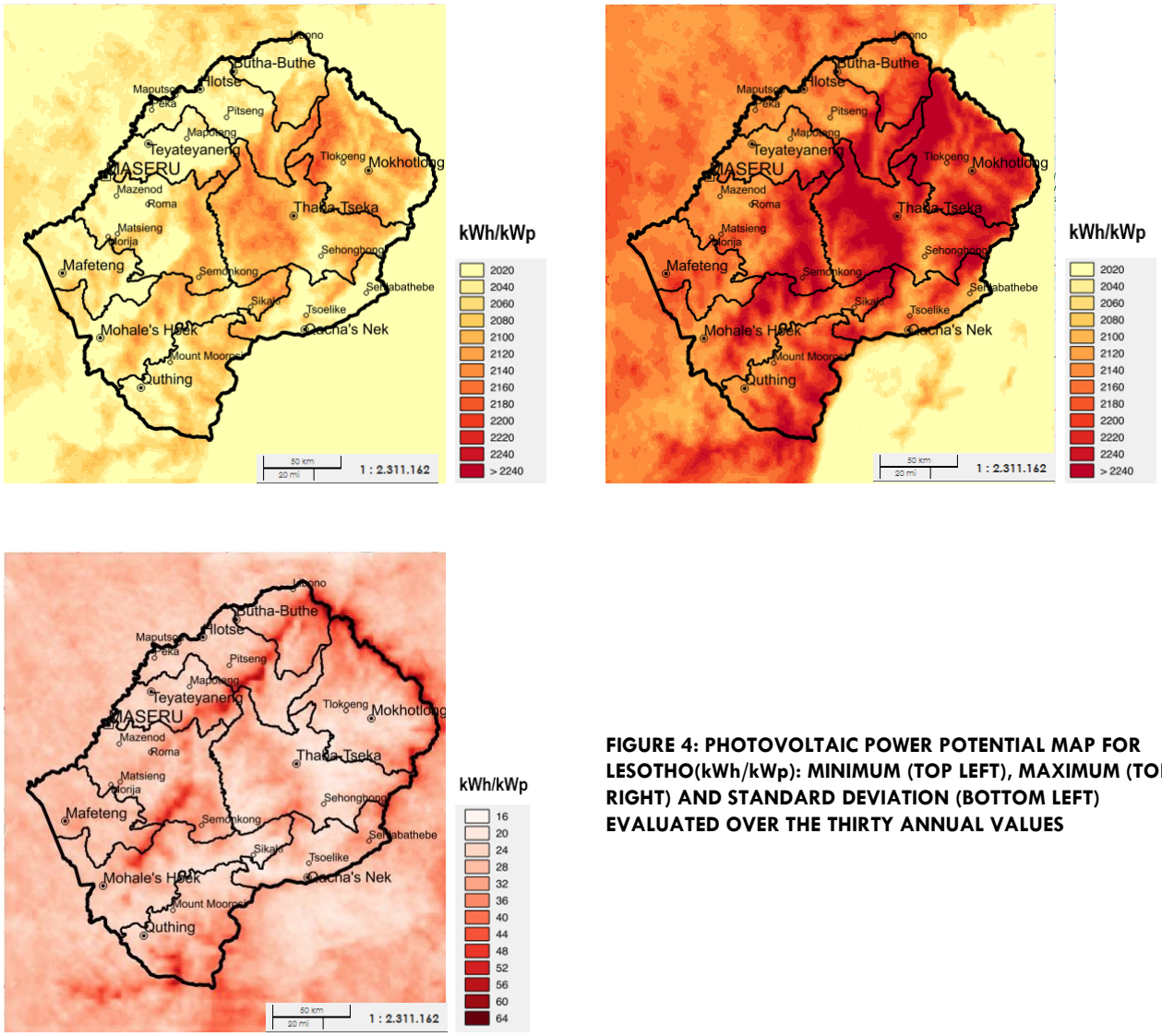

FIGURE 4: PHOTOVOLTAIC POWER POTENTIAL MAP FOR LESOTHO(kWh/kWp): MINIMUM (TOP LEFT), MAXIMUM (TOP RIGHT) AND STANDARD DEVIATION (BOTTOM LEFT) EVALUATED OVER THE THIRTY ANNUAL VALUES

3.3 Additional products for WebGIS

The mean photovoltaic power potential map for Lesotho, along with its inter-annual variability, represents the final outcome of this Work Package. Anyway, several additional products were computed in the framework of the Project and made available into the WebGIS Data Base (deliverable WP4.D2). First of all, as described in Figure 2, global solar radiation on an optimally tilted surface (G in section 3.1.1) was evaluated as well, according to the same workflow (from hourly to period evaluation) depicted for photovoltaic power assessment. Moreover, for both global solar radiation G and photovoltaic power output P, heatmaps were produced, for each point of the

domain, in order to investigate daily modulation and yearly variability of energy assessment. These additional products will be described in the following sections.

3.3.1 Global solar radiation map

Figure 5 and Figure 6 present the average, minimum, maximum and standard deviation fields of the annual global solar radiation on an optimally tilted surface, evaluated over the thirty years period. Again the same classification could be used for average, minimum and maximum maps, pointing out that, in line with PV power outcomes, the same range of values can describe both spatial and inter-annual variability. All the three maps show the highest values located in the highlands in particular in the Thaba Tseka district. Lower values are observed in the foothills and then radiation increases again in the lowlands.

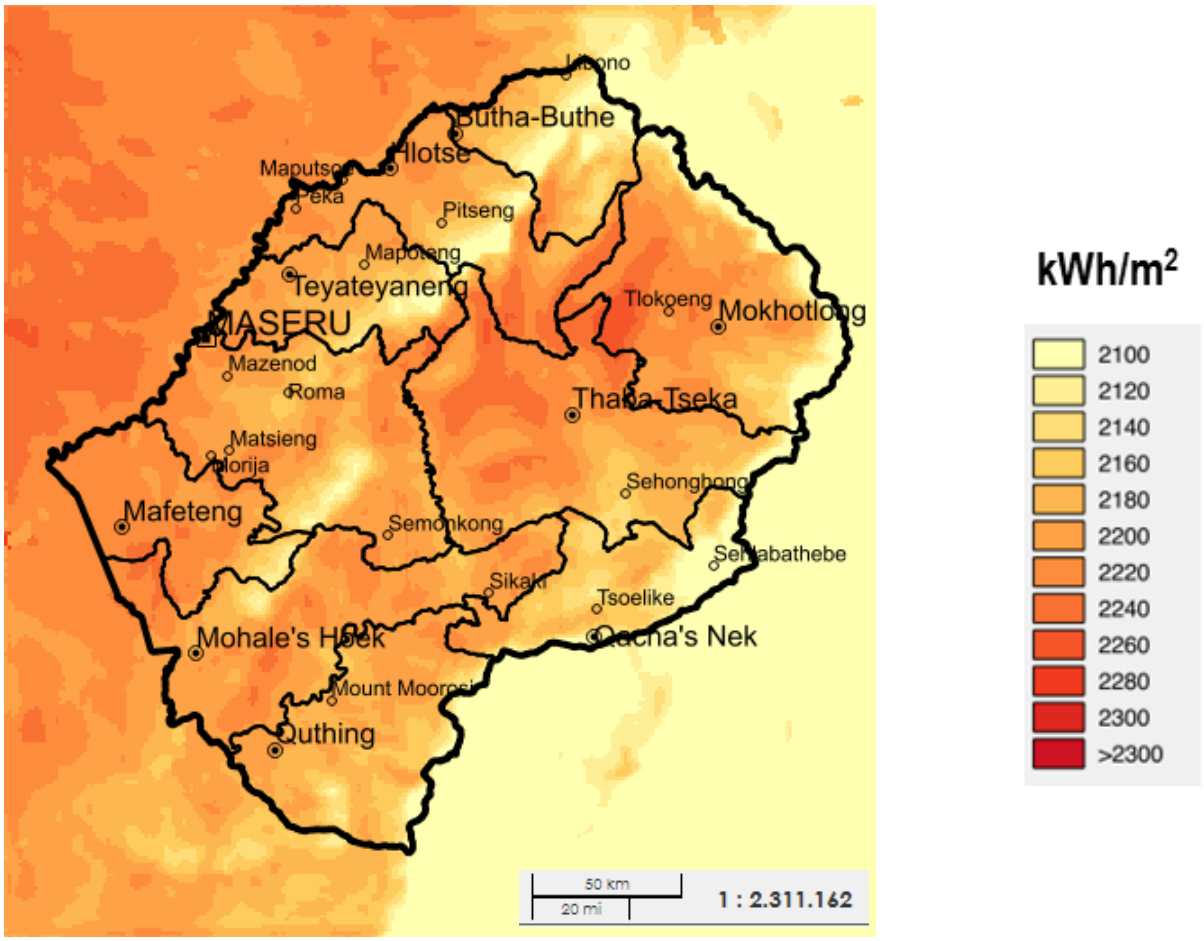

FIGURE 5: AVERAGE GLOBAL SOLAR RADIATION ON AN OPTIMALLY TILTED SURFACE (kWh/m²)

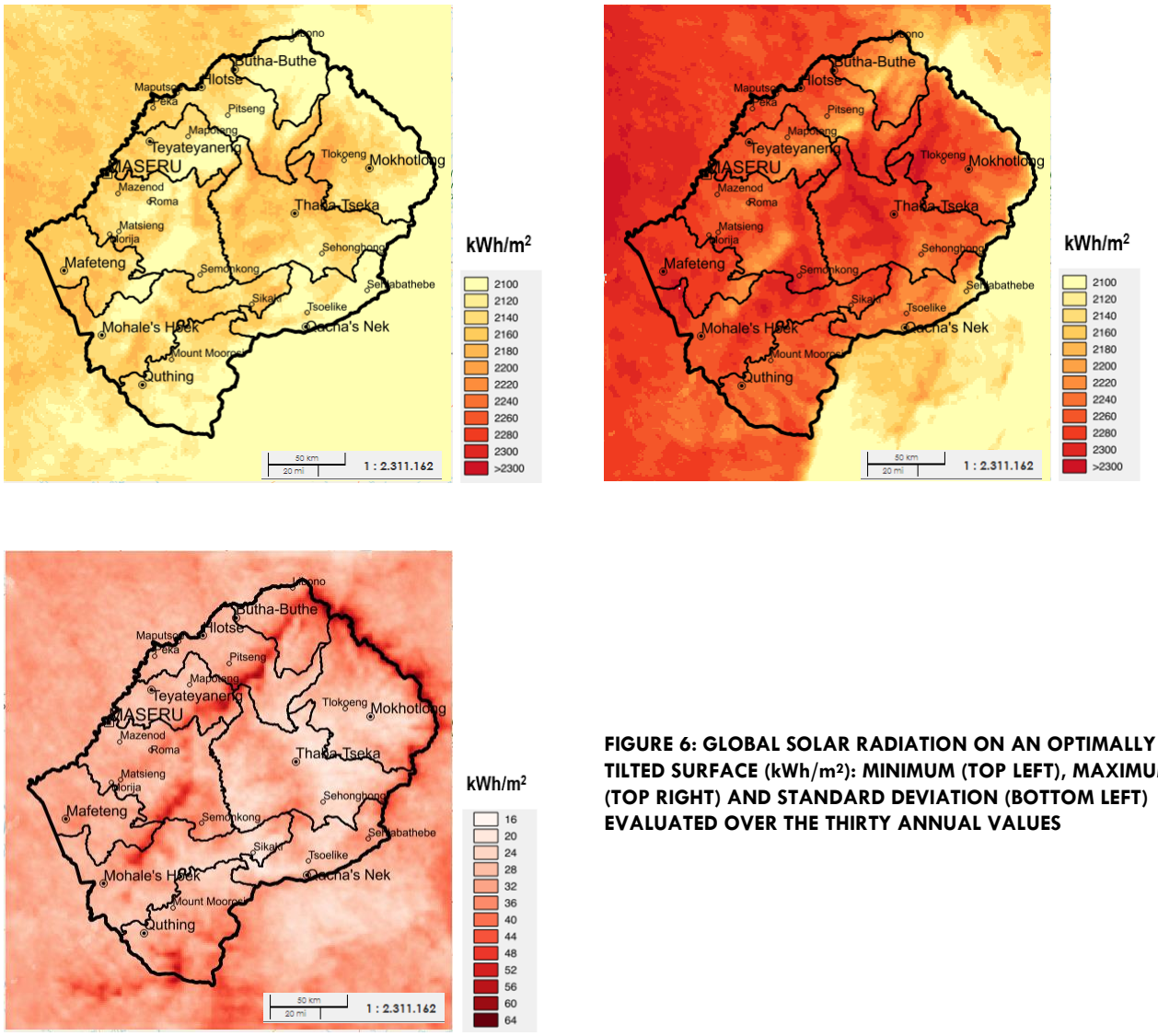

FIGURE 6: GLOBAL SOLAR RADIATION ON AN OPTIMALLY TILTED SURFACE (kWh/m²): MINIMUM (TOP LEFT), MAXIMUM (TOP RIGHT) AND STANDARD DEVIATION (BOTTOM LEFT) EVALUATED OVER THE THIRTY ANNUAL VALUES

The low inter-annual variability is confirmed by the low values of standard deviation outcomes, shown in bottom left panel of Figure 6. In the context of general low values, the higher variability turned out to be located in the foothills area and in the north-east boundary of the country, as it is the case for photovoltaic power.

3.3.2 Global solar radiation and photovoltaic power output heatmaps

Another way to summarize the results was made available into the WebGIS Data Base: heatmaps plots for both global solar radiation and photovoltaic power output were elaborated too.

An heatmap is a graphical representation of any kind of data where values are depicted on a coloured scale starting from the best to the worst element in your ranking of data.

Heatmaps were elaborated, starting from the most detailed data set, i.e the hourly one available as time-varying bi-dimensional fields. Given a grid point *(x,y)*, *G(x,y,t)* and *P(x,y,t)* values were averaged over thirty years, for every hour of the day and for every day of the year. So, for every point *(x,y)* of the grid domain, an heatmap was obtained, consisting in a bi-dimensional plot where an hourly value, computed as an average over thirty years, is associated to every combination (hour of the day, day of the year).

As an example, in Figure 7 the heatmaps outcomes at Maseru position are shown for both global solar radiation (top) and photovoltaic power output (bottom). The patterns clearly give a visual insight of daily and yearly modulations along with the quick identification of the period of both the year and the day with maximum insulation conditions. During the day the highest values are obviously expected close noon. During the year at Maseru position the highest values turn out to be obtained mainly in the months of August and September.

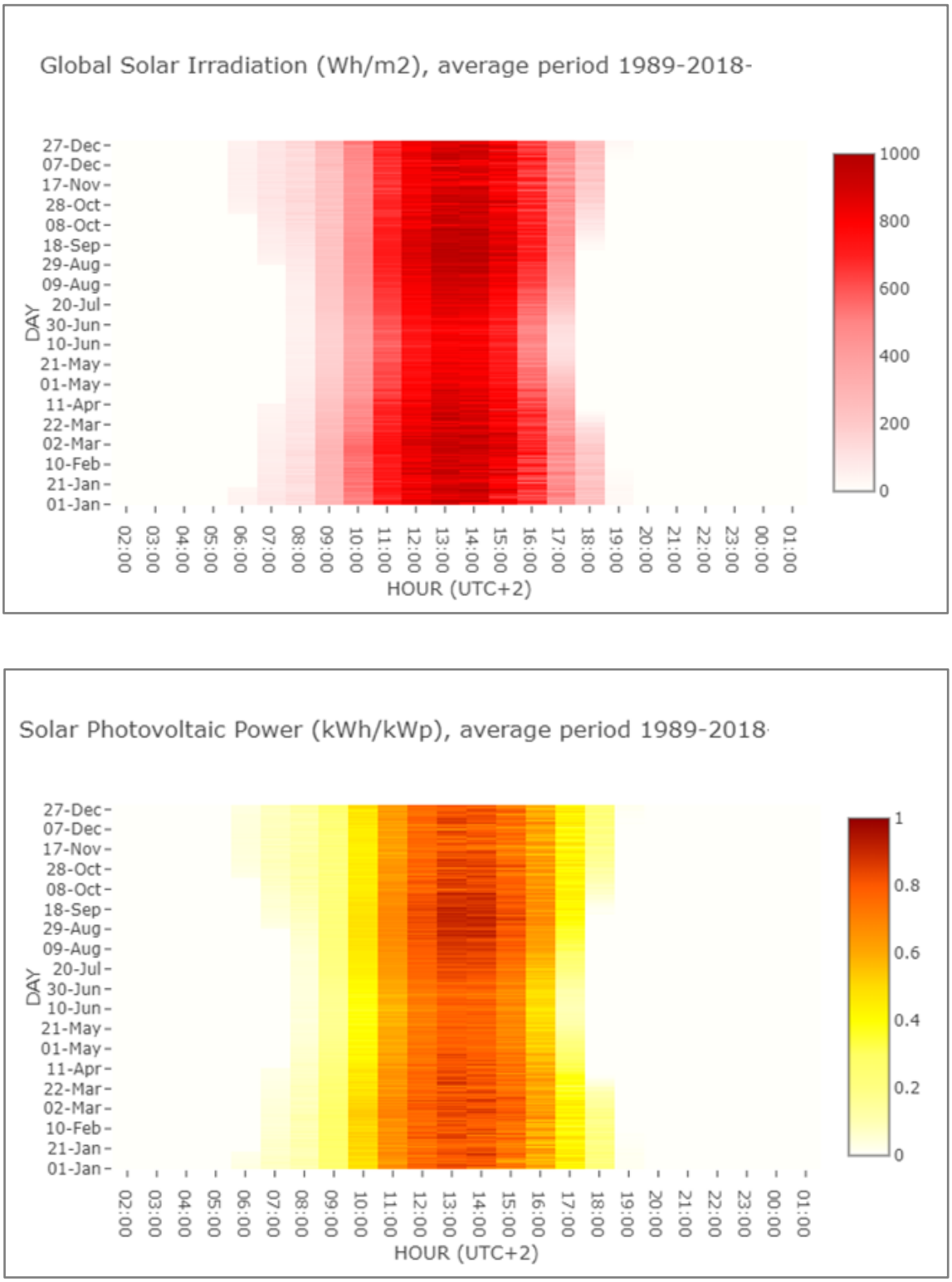

FIGURE 7: HEATMAPS FOR GLOBAL SOLAR RADIATION (TOP) AND PHOTOVOLTAIC POWER OUTPUT (BOTTOM) EXAMPLES AT MASERU POSITION

3.4 Optimal module inclination assessment

In the framework of this Work Package the optimal inclination (β) of the modules, maximizing the annual energy production of the PV system, was investigated too.

Empirically this value is commonly set very close to the latitude (for Lesotho around 29°). Here an optimization procedure was applied using a similar approach to what described in Huld *et al.* (2010). The best inclination of the modules, maximizing the annual energy production, was investigated by calculating power output (P) fields for each of fifteen β values, ranging from 25° to 39°. A step of 1° was used, being 1° accuracy more than sufficient, as stated by Huld *et al.* (2010). For every grid point comparison of the fifteen energy production values, corresponding to the different β values, was made in order to identify the optimum β value for each grid point. As a result a bi-dimensional field of optimum β values was produced to be used for optimal photovoltaic energy assessment.

This outcome was used as an input data (in the equations of sections 3.1.1 and 3.1.5) for the production of the final solar radiation map for Lesotho. Moreover it represents an additional product made available in the framework of the Project: an evaluation, for every grid point of the domain, of the best panel inclination to be used for future PV installation.

In Figure 8 the map of the optimum β values over Lesotho country is presented. Optimum β values mainly range from 28° to 31° over the country and are consistent with latitude variation: as expected, lower values are obtained in the North and higher ones in the South. However, the optimization procedure (based on a robust statistical analysis, i.e. thirty years meteorological data) makes it possible to catch also the influence of the orography and of the typical meteorological conditions (frequently cloudy or not). For example, the eastern part of the domain is characterized by a relatively higher cloud cover, therefore the optimal β values must be smaller, in order to capture more diffuse radiation.

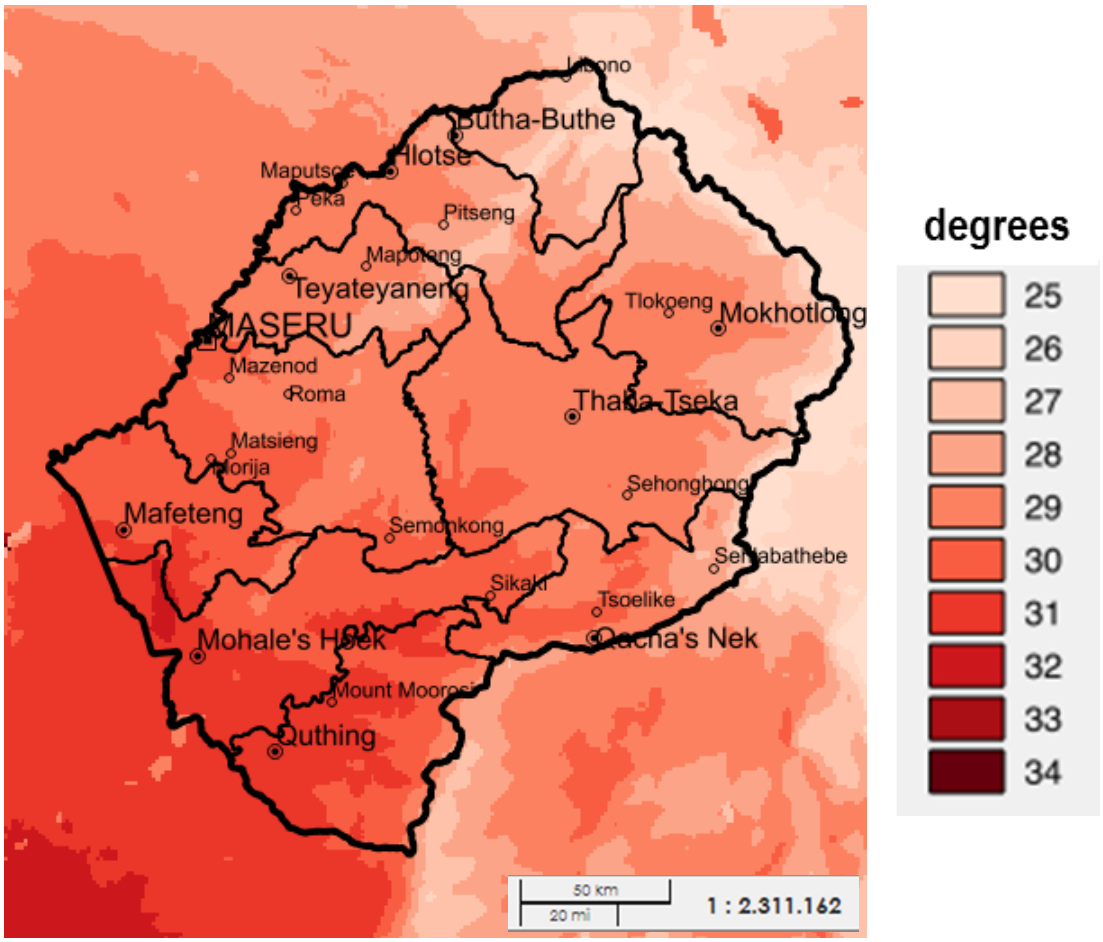

FIGURE 8: MAP OF THE OPTIMUM β VALUES OVER LESOTHO COUNTRY (degrees)

4 CONCLUSIONS

In this report the final outcome of the Work Package WP2 “Solar radiation map for Lesotho” is presented.

In order to capture the more recent climatology and to represent the inter-annual variability of the solar radiation potential, a very long period (thirty years, from 1989 to 2018) was simulated with WRF and PV energy assessment was carried out with the same spatial and temporal both coverage and resolution. Indeed, the energy assessment elaborations could rely on a recent, wide and very detailed meteorological data set.

The final WP2 outcome represents the first assessment of solar photovoltaic energy potential over Lesotho at high horizontal resolution (1 km), based on the state-of-the-art atmospheric model WRF. Results highlighted that Lesotho has a good photovoltaic potential countrywide, ranging from about 2020 to 2240 kWh/kWp. The highest and the lowest values are expected in the highlands and in the foothills, respectively, even if a low variability is observed countrywide.

The final printouts of the solar photovoltaic potential maps were delivered to the Department of Energy at the end of February 2020 together with the wind energy potential maps (WP1.D3), the hydrological map (WP3.D3) and the WebGIS tool (WP4.D2). This set of products is intended to support Lesotho energy planners and policy makers to better address renewable energy exploitation in the country and to help accelerate the transition towards renewable energies, in order to better ensure energy security and to facilitate the road to a low emission development future.

5 BIBLIOGRAPHY

Dubey, S., Sarvaiya, J. N. and Seshadri, B. (2013) 'Temperature dependent photovoltaic (PV) efficiency and its effect on PV production in the world - A review', *Energy Procedia*, 33, pp. 311–321. doi: 10.1016/j.egypro.2013.05.072.

European Centre for Medium Range Weather Forecasts (2020) *ERA5*. Available at: https://www.ecmwf.int/en/forecasts/datasets/reanalysis-datasets/era5 (Accessed: 1 April 2020).

Evans, D. L. and Florschuetz, L. W. (1977) 'Cost studies on terrestrial photovoltaic power systems with sunlight concentration', *Solar Energy*, 19(3), pp. 255–262. doi: 10.1016/0038-092X(77)90068-8.

Faiman, D. (2008) 'Assessing the outdoor operating temperature of photovoltaic modules', *Progress in Photovoltaics: Research and Applications*, 16(4), pp. 307–315. doi: 10.1002/pip.813.

De Felice, M. *et al.* (2019) 'Scoping the potential usefulness of seasonal climate forecasts for solar power management', *Renewable Energy*. Elsevier Ltd, 142, pp. 215–223. doi: 10.1016/j.renene.2019.03.134.

Friesen, G. *et al.* (2007) 'Intercomparison Of Different Energy Prediction Methods Within The European Project "Performance" - Results Of The 1st Round Robin', *22nd European Photovoltaic Solar Energy Conference*, (September), pp. 3–7.

La Gennusa, M. *et al.* (2007) 'A model for managing and evaluating solar radiation for indoor thermal comfort', *Solar Energy*, 81(5), pp. 594–606. doi: 10.1016/j.solener.2006.09.005.

Haupt, S. E. *et al.* (2018) 'Building the Sun4Cast System: Improvements in Solar Power Forecasting', *Bulletin of the American Meteorological Society*. American Meteorological Society, 99(1), pp. 121–136. doi: 10.1175/bams-d-16-0221.1.

Huld, T. *et al.* (2010) 'Analysis of one-axis tracking strategies for PV systems in Europe', *Progress in Photovoltaics: Research and Applications*, 18(3), pp. 183–194. doi: 10.1002/pip.948.

Huld, T. *et al.* (2011) 'A power-rating model for crystalline silicon PV modules', *Solar Energy Materials and Solar Cells*, 95(12), pp. 3359–3369. doi: 10.1016/j.solmat.2011.07.026.

Huld, T. and Gracia Amillo, A. M. (2015) 'Estimating PV module performance over large geographical regions: The role of irradiance, air temperature, wind speed and solar spectrum', *Energies*. MDPI AG, 8(6), pp. 5159–5181. doi: 10.3390/en8065159.

Jimenez, P. A. *et al.* (2016) 'WRF-SOLAR: Description and clear-sky assessment of an augmented NWP model for solar power prediction', *Bulletin of the American Meteorological Society*, 97(7), pp. 1249–1264. doi: 10.1175/BAMS-D-14-00279.1.

Jordan, D. C. and Kurtz, S. R. (2013) 'Photovoltaic degradation rates - An Analytical Review', *Progress in Photovoltaics: Research and Applications*, 21(1), pp. 12–29. doi: 10.1002/pip.1182.

JRC (2020) *European Commission Joint Research Centre*. Available at: https://ec.europa.eu/jrc/en/PVGIS/docs/methods (Accessed: 13 March 2020).

King, D. L., Kratochvil, J. a and Boyson, W. E. (2004) 'Photovoltaic array performance model', *Online*, 8(December), pp. 1–19. doi: 10.2172/919131.

Koehl, M. *et al.* (2011) 'Modeling of the nominal operating cell temperature based on outdoor weathering', *Solar Energy Materials and Solar Cells*, 95(7), pp. 1638–1646. doi: 10.1016/j.solmat.2011.01.020.

Ladwig, W. (2017) 'wrf-python (Version 1.3.2) [Software]'. UCAR/NCAR. doi: 10.5065/D6W094P1.

Lee, J. A. *et al.* (2017) 'Solar irradiance nowcasting case studies near sacramento', *Journal of Applied Meteorology and Climatology*, 56(1), pp. 85–108. doi: 10.1175/JAMC-D-16-0183.1.

Liu, B. Y. H. and C. Jordan, R. (1962) 'Daily insolation on surfaces tilted towards equator', *Transactions ASHRAE*, 67, pp. 526–541.

Maleki, S. A. M., Hizam, H. and Gomes, C. (2017) 'Estimation of hourly, daily and monthly global solar radiation on inclined surfaces: Models re-visited', *Energies*, 10(1). doi: 10.3390/en10010134.

Martin, N. and Ruiz, J. M. (2002) 'Calculation of the PV modules angular losses under field conditions by means of an analytical model', *Fuel and Energy Abstracts*, 43(4), p. 269. doi: 10.1016/s0140-6701(02)86350-0.

Martin, N. and Ruiz, J. M. (2013) 'Corrigendum to "Calculation of the PV modules angular losses under field conditions by means of an analytical model" [Sol. Energy Mater. Sol. Cells 70 (1) (2001) 25–38] (S0927024800004086) (10.1016/S0927-0248(00)00408-6))', *Solar Energy Materials and Solar Cells*, 110, p. 154. doi: 10.1016/j.solmat.2012.11.002.

National Centre for Atmospheric Research (NCAR) (2014) 'ARW Version 3 Modeling System's User's Guide'. Boulder: NCAR.

Ponti, G. *et al.* (2014) 'The role of medium size facilities in the HPC ecosystem: The case of the new CRESCO4 cluster integrated in the ENEAGRID infrastructure', in *Proceedings of the 2014 International Conference on High Performance Computing and Simulation, HPCS 2014*, pp. 1030–1033. doi: 10.1109/HPCSim.2014.6903807.

Reis, F. *et al.* (2010) 'Modeling the performance of low concentration photovoltaic systems', *Solar Energy Materials and Solar Cells*, 94(7), pp. 1222–1226. doi: 10.1016/j.solmat.2010.03.010.

Skamarock, W. C. and Klemp, J. B. (2008) 'A time-split nonhydrostatic atmospheric model for weather research and forecasting applications', *Journal of Computational Physics*. Academic Press Inc., 227(7), pp. 3465–3485. doi: 10.1016/j.jcp.2007.01.037.

Skoplaki, E. and Palyvos, J. A. (2009) 'Operating temperature of photovoltaic modules: A survey of pertinent correlations', *Renewable Energy*. Elsevier BV, 34(1), pp. 23–29. doi: 10.1016/j.renene.2008.04.009.

Zender, C. S. (2008) 'Analysis of self-describing gridded geoscience data with netCDF Operators (NCO)', *Environmental Modelling and Software*, 23(10–11), pp. 1338–1342. doi: 10.1016/j.envsoft.2008.03.004.